2020 25th International Conference on Pattern Recognition (ICPR)
Milan, Italy, Jan 10-15, 2021

Can you really trust the sensor's PRNU? How image content might impact the finger vein sensor identification performance

Dominik Söllinger, Luca Debiasi and Andreas Uhl
Department of Computer Science
University of Salzburg
Jakob-Haringer-Str. 2, 5020 Salzburg, Austria
{dsoellinger, ldebiasi, uhl} @cs.sbg.ac.at

***Abstract*—We study the impact of highly correlated image content on the estimated photo response non-uniformity (PRNU) of a sensor unit and its impact on the sensor identification performance. Based on eight publicly available finger vein datasets, we show formally and experimentally that the nature of finger vein imagery can cause the estimated PRNU to be biased by image content and lead to a fairly bad PRNU estimate. Such bias can cause a false increase in sensor identification performance depending on the dataset composition. Our results indicate that independent of the biometric modality, examining the quality of the estimated PRNU is essential before the sensor identification performance can be claimed to be good.**

I. Introduction

In the field of digital image forensic the photo response non-uniformity (PRNU) of an imaging sensor has emerged as an important tool for various forensic tasks like device identification, device linking or the detection of digital forgeries. Inhomogeneity of silicon wafers and imperfections introduced during the sensor manufacturing process cause varying sensitivity of each pixel to light. The consequence is a sensor-specific, noise-like pattern termed PRNU which is an intrinsic property of the sensor and present in every image.

However, besides its applicability for forensic tasks in general, the PRNU also turned out to be useful in the biometric context. A common example is the detection of a fabricated biometric trait that could have been injected at many points within a biometric system. As fabricated biometric data can be expected to exhibit a different PRNU than the source sensor, PRNU-based sensor identification can be use to detect fabricated data. In biometrics, most work in the field of sensor identification deals with iris [1], [2], [3], [4], [5], [6] and fingerprint sensors [7]. Most of the work confirms that PRNU-based approaches are well-suited for sensor identification, only in [5], [6] considerably fluctuating equal error rates and thresholds depending on the sensor were reported.

More recently, researchers studied the applicability of PRNU-based sensor identification for finger vein imagery and investigated which regions work best for sensor identification [8]. The outcome was that PRNU-based sensor identification works well for finger vein imagery but regions that contain biometric trait (finger vein tissue) should be preferred over background regions. The authors justified the poor performance of background regions by the fact that the image content is highly correlated in such regions.

However, in theory, extracted noise residuals should always be independent of the image content. Consequently, if correlated content caused the poor performance, noise residuals would have to be strongly contaminated with structures directly inferred from the image content and the estimated fingerprint be a poor estimate of the true sensor PRNU. In addition to that, we would expect to see a false increase in sensor identification performance considering the nature of publicly available finger vein datasets and the fact that images of a dataset are typically captured with the same sensor. In other words, there is a risk of mixing up sensor identification with a task better referred as "dataset identification".

To better understand the problem simply consider a dataset composed of visually similar-looking images captured with two different sensors. In such case, the sensor identification performance can be expected to be low if the estimated PRNU is heavily biased by the image content as it is impossible to identify the source sensor based on the image content. However, if all images are captured with the same sensor — to the best of our knowledge, this is the case for all publicly available finger vein datasets available at this point — there is risk of achieving a good identification performance although the classification is based on image content rather than the PRNU.

In this work, we evaluate the impact of image content on a sensor unit's estimated PRNU in the context of finger vein imagery. More precisely, we test whether the sensor identification performance in image regions with characteristic, dataset-specific structures outperforms regions without such structures. Strong performance differences may indicate a strongly biased PRNU and that we should be careful about the real sensor identification performance. To develop an understanding of how crucial this effect might be, we then analyze how image denoising changes the correlation between residuals and the estimated PRNU. As denoising destroys the residual information and therefore the sensor PRNU, the image content can be expected to have a huge effect on the identification performance if the PRNU still strongly correlates with the residuals in case of

978-1-7281-8808-9/20/$31.00 ©2020 IEEE

denoised images.

Note that although this work has been conducted in the context of finger veins, our findings can be equally transferred to other biometric modalities. In fact, simple due to the nature of biometric image acquisition where stable acquisition conditions are typically desirable, it's not unlikely that we encounter highly correlated image content. As a result, it's highly probable that similar observation can be made for other biometric modalities as well.

II. Estimating the sensor PRNU

A commonly used method for constructing the sensor PRNU was proposed by Fridrich in [9]. For a set of N grayscale images $\{I_1, ..., I_N\} \in \mathbb{R}^{w \times h}$ taken by the same sensor, the idea is to first extract the residual noise matrix $W_k \in \mathbb{R}^{w \times h}$ for each image I_k where $k \in \{1, ..., N\}$ as shown in Eqn. 1. $I_k^{(0)} \in \mathbb{R}^{w \times h}$ denotes the "true scene" image that would be captured in the absence of imperfections/distortions such as dark current, shot noise, etc.

$$W_k = I_k - I_k^{(0)} \tag{1}$$

The sensor PRNU K can then be estimated using MLE (Maximum Likelihood Estimation) as shown in Eqn. 2. Note that all matrix operations are understood element-wise.

$$\hat{K} = \frac{\sum_{k=1}^{N} W_k I_k}{\sum_{k=1}^{N} {I_k}^2} \tag{2}$$

The challenge though is that $I_k^{(0)}$ is unknown in practice and can only be approximated by $F(I_k)$ where F is some denoising function. Various denoising functions have been proposed to allow $I_k^{(0)} \approx F(I_k)$. Examples for such denoising function include the denoiser proposed by Lukas in Appendix A of [10], Mihcak et al. in [11] and BM3D by Dabov et al. in [12]. Additionally, a lot of effort went into the development of enhancement techniques to improve the estimated residual noise W_k.

III. About the difficulty of PRNU extraction for finger vein imagery

Despite the availability of different denoising methods optimized for residual noise extraction, the quality of the estimated PRNU can be shown to heavily depend on the image content in strongly textured regions and around edges (regions with non-smooth image content). This can be easily seen by comparing the nature of regions with smooth/non-smooth image content in the frequency domain. Due to the inability of the denoising filter to separate content from noise perfectly, the remnant of the image content in $I_k - F(I_k)$ will be relatively large in non-smooth regions due to structures, such as edges, being confused with noise. In smooth regions, though, it will be relatively small. For this very reason, [9] already stated that images with high luminance and smooth content should be prefered for PRNU estimation.

Considering the nature of publicly available finger vein datasets, it can be seen that the assumption of "smooth image content" only holds for some subregions in the image. A closer look at the sample images in Fig. 1 unveils that most datasets exhibit what we refer to as *regions with characteristic structures*. These are regions with edge-like structures, such as the finger positioning apparatus or a prominent illumination pattern, which are present in every single image of a dataset and positionally stable (always appear at the same location in the image), a.k.a. highly correlated image content.

To better understand the impact of such structures on the PRNU estimate, we have to take a look on how Eqn. 2 is derived in [9] and what assumptions are made during this process. We therefore first look at the definition of the model for the residual noise W_k where the term $\Xi_k \in \mathbb{R}^{n \times m}$ represents the sum of all noise/error components of the image I_k (such as the dark current, offset or content leftover in $I_k - F(I_k)$).

$$\begin{aligned} W_k &= I_k - F(I_k) \\ &= I_k K + \Xi_k \end{aligned} \tag{3}$$

For the derivation of the ML estimator, it is then assumed that the content leftover in $I_k - F(I_k)$ in Ξ_k is small compared the signal $I_k K$ and Ξ_k can be therefore considered as independent of $I_k K$.

However, as we already observed before, the assumption that the content leftover is small does not apply for areas with characteristic structures in finger vein images. As a result, it is unreasonable to model Ξ_k by WGN (White Gaussian Noise) as proposed in [9]. Things get even worse if we take into account that our characteristic structures recur in every image. To make this problem more obvious we denote the content leftover in $I_k - F(I_k)$ as Ψ_k and exclude it from the term Ξ_k. The resulting model is shown in Eqn. 4. In this new model, the assumption that Ξ_k can be modeled by WGN is again reasonable.

$$W_k = I_k K + \Xi_k + \Psi_k \tag{4}$$

Eqn. 4 can then be rewritten to Eqn. 5 by element-wise division through I_k.

$$\frac{W_k}{I_k} = \left(K + \frac{\Psi_k}{I_k}\right) + \frac{\Xi_k}{I_k} \tag{5}$$

As can be seen in Eqn. 5, we now find the term $\frac{\Psi_k}{I_k}$ to directly bias the PRNU K as additive component. Additionally, we can expect $\frac{\Psi_k}{I_k}$ to be large (and almost constant!) in regions with characteristic structures. As a result, it can be concluded that the estimated PRNU (Eqn. 2) will be heavily biased by the image content in regions with characteristic structures.

IV. Experimential Design

As the primary goal in this work was to understand the impact of the image content on the PRNU fingerprint quality, we decided to compare the PRNU-based sensor identification performance in different image regions, each region exhibiting different types of image content and properties (see Sec. IV-B).

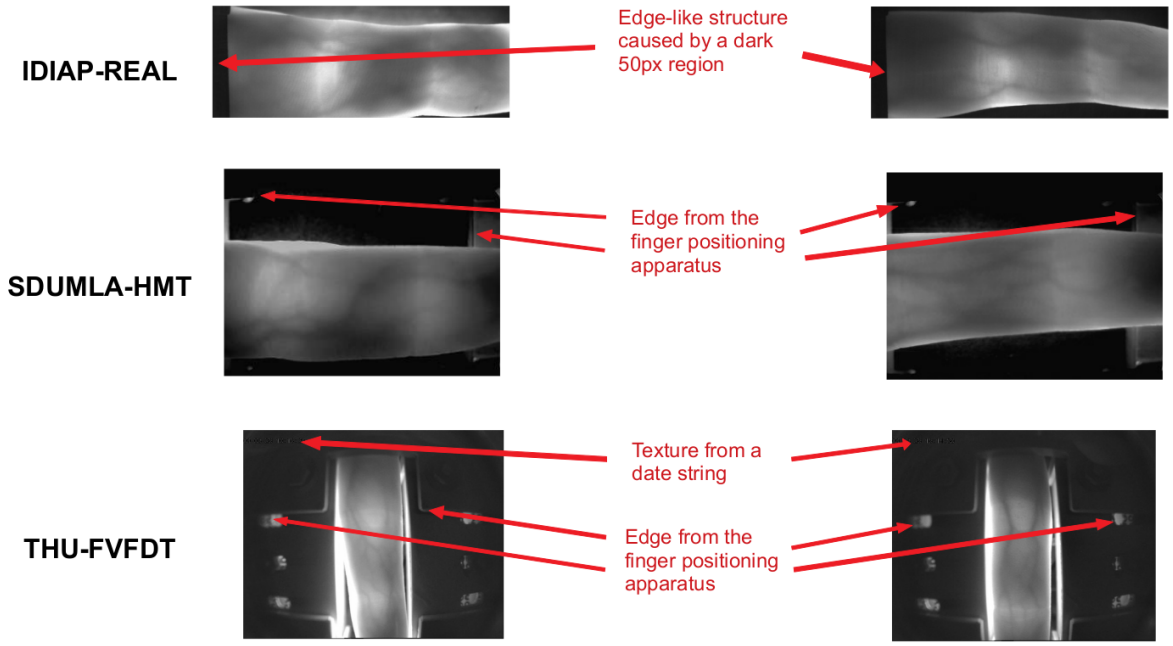

Fig. 1. Sample images of four different finger vein datasets. The arrows mark sample regions which we expect to exhibit *characteristic structures*. Typically these are prominent edge-like structures that are occur at the same position in every image of a dataset.

We then repeated these experiments using different state-of-the-art denoisers as well as enhancement methods.

Note that, if your assumption holds, we expect PRNUs generated from regions with characteristic, (partially) stable structures to (falsely!) outperform regions without such structures in sensor identification.

A. Datasets

All tests were conducted with the following publicly available datasets. For each dataset we composed equally sized subsets of 120 images. Note that, after checking the dataset descriptions and corresponding literature, we agreed to assume that a single sensor unit was used to capture all images of a dataset. However, we could not explicitly verify that this is the case (e.g., based on image metadata).

- **SDUMLA-HMT** [13] - Images are stored in BMP format with 320×240 pixels in size. Our composed subset consists of images of index, middle and ring fingers (one image / finger) taken from the first 20 subjects in the dataset.
- **IDIAP VERA (IDIAP-REAL)** [14] - Images are stored in PNG format with a size of 250×665 pixels. Our composed subset consists of images of the left and right index finger taken from the first 60 subjects.
- **FV-USM** [15] - Images of the dataset are stored in JPEG format with a size of 480×640 pixels. Our composed subset consists of images of the four fingers (one image / finger) taken from the first 30 subjects.
- **MMCBNU_6000 (MMCBNU)** [16] - Images are stored in BMP format with a size of 640×480 pixels. Our composed subset consists of one images of each finger taken from the first 20 subjects.
- **PLUS-FV3-Laser-Palmar (Palmar)** [17] - Images are stored in PNG format with a size of 600×1024 pixels. Our composed subset consists of one image from each finger taken from the first 20 subjects.
- **THU-FVFDT** [1] - Images are stored in BMP format with a size of 720×576 pixels. Our composed subset consists of all images taken from the first 120 subjects.
- **UTFVP** [18], [19] - Images are stored in PNG format with a size of 672×380 pixels. Our composed subset consists of images taken from the first 20 subjects.
- **HKPU-FV** [20] - Images are stored in BMP format with a size of 513×256 pixels. Our composed subset consists of one image of both fingers taken from the first 60 subjects.

B. Image regions and properties

For each dataset, we manually defined a set of equally sized image regions (50 × 50 pixels) and manually categorized them into one out of five region types by carefully examining each region's image content. Of course, the choosing the right categorization was often a rather subjective thing. A good way of determining the best region type turned out to be by looking at the content of the PRNU fingerprint.

Region Types:

- **Fingervein (FV)** - Region mostly contains finger vein tissue

[1] https://www.sigs.tsinghua.edu.cn/labs/vipl/thu-fvfdt.html

- **Background (BG)** - Mostly contains strongly varying non-finger vein content. No characteristic structures (e.g. edges).
- **Static (ST)** - Contains a characteristic structure that occurs at the same pixel position in each image.
- **Semi Static (SS)** - Contains a characteristic structure but its location varies slightly in every image
- **All Black (AB)** - No image content. Pixels are uniformly black in almost every image. PRNU estimation is almost impossible.

A visualization of all chosen crop regions can be seen in Fig. 2. Please make sure to have a color copy of this work when looking at the figure since region types are color-coded.

C. Workflow

We started by choosing one of the eight finger vein datasets as the "Sensor PRNU" dataset and applied subject-wise 4-fold cross-validiation to partition the dataset into 4 folds (30 images/fold) by splitting the images based on their subject ids. We then used the images of 3 folds (90 images) as the training set to estimate the sensor PRNU. The images in the remaining fold (30 images) were joint with the images of the remaining datasets (7×120 images) to form the test set.
For PRNU estimation and residual extraction we applied the method described in Sec. II together with different PRNU/residual enhancement methods and denoising filters proposed in literature. An overview of the different "enhancement modes" can be found in Table I. For further details on the PRNU/residual enhancement methods please consider reading the work referenced in the table caption.
After estimating the sensor PRNU we calculated the match score $\rho_{[R_I,I_QK]}$ as shown in Eqn. 6 for all different region combinations by cropping the corresponding image region from the sensor PRNU K as well as the query image I_Q and query image residual R_I from the test set. NCC denotes the normalized cross correlation.

$$\rho_{[R_I,I_QK]} = NCC(R_I, I_QK) \tag{6}$$

This process was then repeated for all 4 folds and datasets.

Finally, each match score can be "linked" to one of the following six region pairs depending on the region types it was calculated from.

Region Pairs:

- **P-FV / FV** - PRNU / residuals from the "Sensor PRNU" dataset are taken from a *FV* region. Residuals of the other datasets are taken from a *FV* region.
- **P-BG-AB / BG-AB** - PRNU / residuals from the "Sensor PRNU" dataset are taken from a *BG* or *AB* region. Residuals of the remaining datasets are taken from a *BG* or *AB* region.
- **P-ST / BG-AB** - PRNU / residuals from the "Sensor PRNU" dataset are taken from a *ST* region. Residuals of the other datasets are taken from a *BG* or *AB* region.
- **P-SS / BG-AB** - PRNU / residuals from the "Sensor PRNU" dataset are taken from a *SS* region. Residuals of the other datasets are taken from a *BG* or *AB* region.
- **P-ST / FV** - PRNU / residuals from the "Sensor PRNU" dataset are taken from a *ST* region. Residuals of the other datasets are taken from a *FV* region.
- **P-SS / FV** - PRNU / residuals from the "Sensor PRNU" dataset are taken from a *SS* region. Residuals of the other datasets are taken from a *FV* region.

V. Experimental Results

A. Identification performance in different image regions

Table II, III and IV show the sensor identification performance for PRNUs generated from the THU-FVFDT, SDUMLA-HMT and IDIAP-REAL dataset. These are the datasets which we identified to have static SS and semi-static ST region types in Sec. IV-B. As in this work we primarily want to study the performance difference between characteristic (static, semi-static) and non-characteristic (non-static) regions, we omit showing results for other "sensor PRNU" datasets in this work. The identification performance is reported as AUC ROC (Area under the Receiver Operating Characteristic curve) score.

The THU-FVFDT identification performance shown in Table II confirms the hypothesis made in Sec. IV. No matter which enhancement methods are applied, the identification performance achieved with PRNUs generated from static *ST* (*P-ST/BG-AB*, *P-ST/FV*) and semi-static *SS* (*P-SS/BG-AB*, *P-SS/FV*) regions largely outperforms the performance of PRNUs generated from finger vein *FV* (*P-FV/FV*) or background *BG-AB* (*P-BG-AB/BG-AB*) regions.

A similar behavior, but not quite as clear as for THU-FVFDT, can be found for SDUMLA-HMT in Table III. Considering the identification performance, PRNUs generated from static *ST* (*P-ST/BG-AB*, *P-ST/FV*) regions again outperform the PRNUs generated from background (*P-BG-AB/BG-AB*) regions. Nevertheless, we can still observe a good identification performance in foreground (*P-FV/FV*) regions. Note that the performance for *P-SS* region pairs (*P-SS/BG-AB*, *P-SS/FV*) could not be evaluated due to the absence of semi-static *SS* regions in the SDUMLA-HMT dataset.

Sensor identification in the case of IDIAP-REAL (Table IV) in general seems to work extremely well. No matter whether which region is taken, the identification performance is almost perfect. Again, *P-SS* region pairs could not be evaluated due to the absence of *SS* regions.

B. Performance comparison of different denoising modalities

Although identifying which denoising modalities (denoising and residual enhancement methods) work best for finger vein imagery was not the primary goal in this work, it is at least worth to point out some interesting observations.

Fig. 3 and 4 show the (sensor-)averaged sensor identification performance for different denoising modalities in the region pairs *FV* and *BG-AB*.

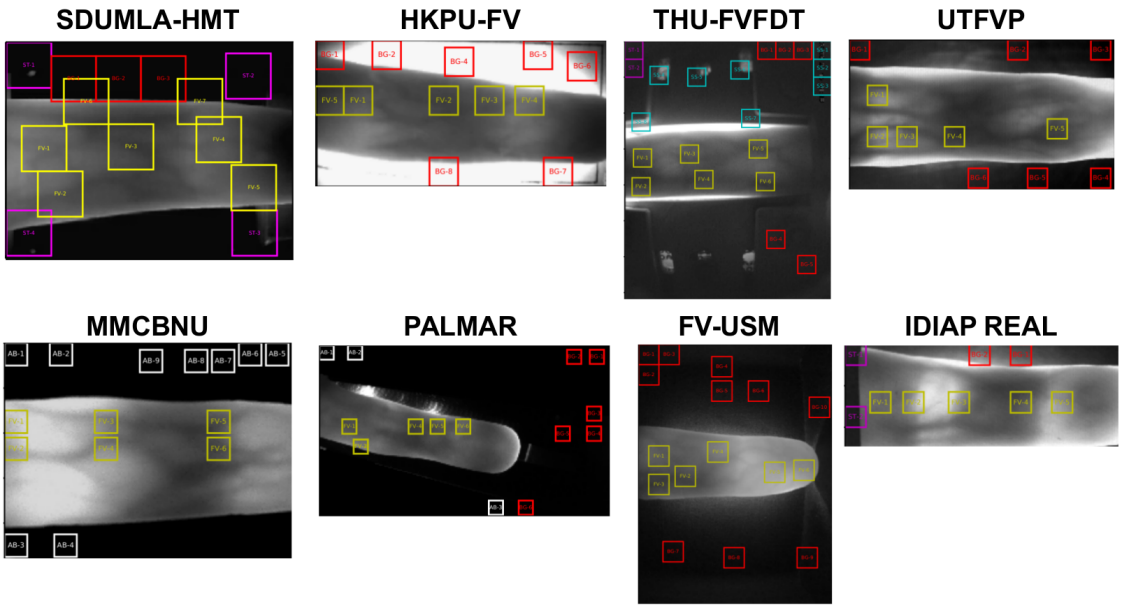

Fig. 2. Visualization of image regions used for each dataset. Different colors represent different region types. Yellow - FV: Finger vein region. Red - BG: Background region. Magenta - ST: Characteristic, positionally stable structures. Cyan - SS: Characteristic structures but not positionally stable. White - AB: Black pixel values only.

Extraction Mode	Denoiser	PRNU Enhancement	PRNU Residual Enhancement	Residual Enhancement
LUKAS	Lukas	Wiener DFT		Wiener DFT
BM3D	BM3D			
LI-3	Mihcak		Li-3	Li-3
LI-5	Mihcak		Li-5	Li-5
CAL	Mihcak		Caldelli	Caldelli
SEA+FDR	Mihcak	SEA	FDR + Li-3	FDR + Li-3

Ref: Lukas [10], Li-3 [21], Li-5 [21], Caldelli [22], FDR [23], SEA [24], Wiener DFT [9], Mihcak [11], BM3D [12]

TABLE I
OVERVIEW OF DIFFERENT ENHANCEMENT MODES

Region Pair	Enhancement Mode					
	LUKAS	*BM3D*	*LI-3*	*LI-5*	*CAL*	*SEA+FDR*
P-FV / FV	0.65 (0.07)	0.80 (0.08)	0.78 (0.09)	0.76 (0.09)	0.75 (0.09)	0.78 (0.06)
P-BG-AB / BG-AB	0.88 (0.10)	0.84 (0.04)	0.92 (0.06)	0.92 (0.07)	0.91 (0.07)	0.86 (0.06)
P-ST / BG-AB	0.99 (0.01)	0.85 (0.10)	0.99 (0.01)	1.00 (0.00)	1.00 (0.01)	0.83 (0.09)
P-ST / FV	1.00 (0.00)	0.94 (0.07)	1.00 (0.00)	1.00 (0.01)	1.00 (0.01)	0.91 (0.06)
P-SS / BG-AB	0.93 (0.11)	0.89 (0.08)	0.95 (0.07)	0.97 (0.06)	0.97 (0.06)	0.95 (0.05)
P-SS / FV	0.94 (0.11)	0.96 (0.06)	0.97 (0.07)	0.97 (0.05)	0.98 (0.05)	0.98 (0.03)

TABLE II
SENSOR IDENTIFICATION PERFORMANCE (AUC ROC) FOR PRNUS ESTIMATED FROM THE THU-FVFDT DATASET

Region Pair	Enhancement Mode					
	LUKAS	*BM3D*	*LI-3*	*LI-5*	*CAL*	*SEA+FDR*
P-FV / FV	0.99 (0.01)	1.00 (0.01)	0.99 (0.02)	0.99 (0.01)	0.99 (0.01)	0.99 (0.02)
P-BG-AB / BG-AB	0.88 (0.14)	0.89 (0.10)	0.90 (0.11)	0.98 (0.02)	0.98 (0.02)	0.85 (0.13)
P-ST / BG-AB	0.99 (0.01)	0.99 (0.01)	0.99 (0.01)	1.00 (0.00)	1.00 (0.01)	0.98 (0.02)
P-ST / FV	1.00 (0.00)	1.00 (0.00)	1.00 (0.00)	1.00 (0.00)	1.00 (0.00)	1.00 (0.01)
P-SS / BG-AB	-	-	-	-	-	-
P-SS / FV	-	-	-	-	-	-

TABLE III
SENSOR IDENTIFICATION PERFORMANCE (AUC ROC) FOR PRNUS ESTIMATED FROM THE SDUMLA-HMT DATASET

Region Pair	Enhancement Mode					
	LUKAS	*BM3D*	*LI-3*	*LI-5*	*CAL*	*SEA+FDR*
P-FV / FV	1.00 (0.00)	1.00 (0.00)	1.00 (0.00)	1.00 (0.00)	1.00 (0.00)	0.99 (0.02)
P-BG-AB / BG-AB	0.97 (0.07)	0.99 (0.01)	1.00 (0.00)	1.00 (0.00)	1.00 (0.00)	0.99 (0.01)
P-ST / BG-AB	1.00 (0.00)	1.00 (0.01)	1.00 (0.00)	1.00 (0.00)	1.00 (0.00)	1.00 (0.00)
P-ST / FV	1.00 (0.00)	1.00 (0.00)	1.00 (0.00)	1.00 (0.00)	1.00 (0.00)	1.00 (0.00)
P-SS / BG-AB	-	-	-	-	-	-
P-SS / FV	-	-	-	-	-	-

TABLE IV
SENSOR IDENTIFICATION PERFORMANCE (AUC ROC) FOR PRNUS ESTIMATED FROM THE IDIAP-REAL DATASET

While it can be seen in Fig. 3 that *BM3D* (0.957) and *SEA+FDR* (0.949) perform best in finger vein regions, exactly the opposite is the case for background *BG-AB* regions in Fig. 4. For the *BG-AB* region pair, *LI-5* (0.860), *CAL* (0.858) and *LUKAS* (0.853) perform best. In general, it's fairly interesting to see that there is a trend for denoising modalities to perform worse in background regions if they perform well in finger vein regions (and vice versa).

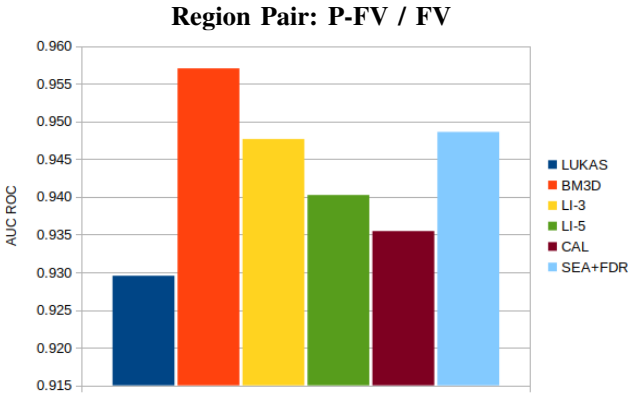

Fig. 3. Average sensor identification performance for region pair *P-FV / FV* using different extraction modes

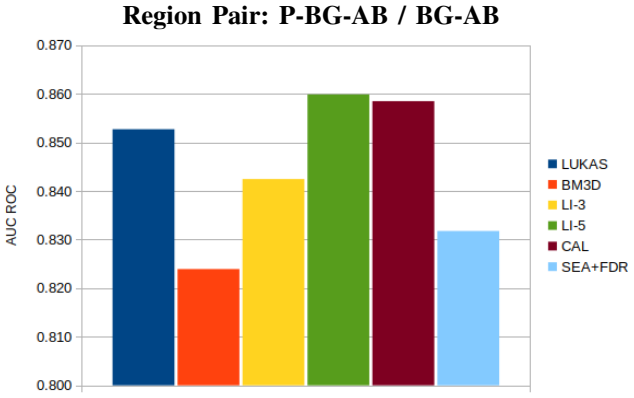

Fig. 4. Average sensor identification performance for region pair *P-BG-AB / BG-AB* using different extraction modes

VI. IMPACT ANALYSIS — WHAT IF WE CHOSE THE WRONG REGION?

The findings described in Sec. V-A provide evidence for the estimated PRNU being biased by image content in regions with characteristic structures. Nevertheless, it's not entirely clear how these contaminations impact the true sensor identification. Keep in mind that images of all datasets used in our experiments were captured with the same sensor and it is therefore difficult to quantify the real-world impact of the contaminations.

To develop an intuition for the criticality of the contaminations we conduct a simple experiment. Assuming that we previously obtained a good estimate of the true sensor PRNU from a given set of images, the correlation with noise residuals extracted from the image set can be expected to be high. However, if we correlate the fingerprint with residuals of denoised image versions, the average correlation score should decrease (be close to 0) because denoising destroys the residual information. However, if the PRNU is contaminated with structures inferred from the image content, the impact of denoising can be expected to be low as most characteristic structures will still be preserved in the denoised image. This indicates that the image content is more important for matching than the residual noise.

To verify whether this is the case, we first estimated the sensor PRNU for each of the eight datasets presented in Sec. IV-A. For each fingerprint, we then calculated the average NCC with residuals extracted from a single (but large) image region which only exhibits finger vein tissue. Similarly, we repeated this process with BM3D-denoised version of the images. Note that, if we only focused on regions that exhibit finger vein tissue, the contamination of the PRNU with characteristic structures can be expected to be low if not non-existent. We then repeated the process using non-cropped (full) images. We expect the overall decrease in identification performance to be much less significant for datasets with characteristic structures.

The results for the described experiment are shown in Table V. As can be seen the relative change in correlation for "Full image" is much lower than for "Finger vein" in case of THU-FVFDT, FV-USM, HKPU-FV and SDUMLA-HMT. Note that with THU-FVFDT and SDUMLA-HMT the list includes exactly those datasets which we assumed to have characteristic structures in Sec. IV-B. It's also interesting to see that in case of THU-FVDT, denoising even causes an increase in identification performance.

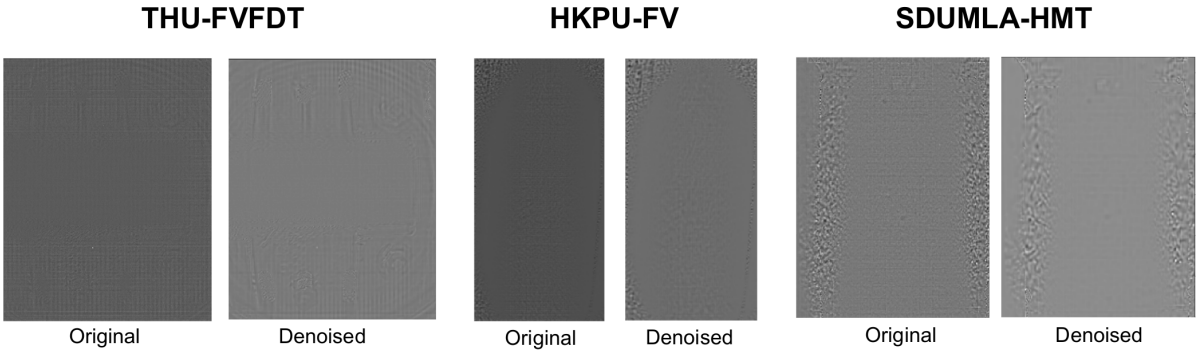

Fig. 5. Comparison of PRNUs obtained from original images with PRNUs from denoised images. As can be seen in the images, characteristic structures (edges) appear more prominent in the denoised versions.

Dataset	Finger vein region			Full (non-cropped) image		
	Original	*Denoised*	*Change*	*Original*	*Denoised*	*Change*
THU-FVFDT	0.11	0.05	↓ 55.7%	0.13	0.14	↑ **05.4%**
FV-USM	0.26	0.10	↓ 60.6%	0.32	0.21	↓ 35.0%
MMCBNU	0.19	0.10	↓ 46.4%	0.20	0.10	↓ 46.7%
PALMAR	0.48	0.11	↓ 77.3%	0.46	0.10	↓ 77.6%
UTFVP	0.73	0.13	↓ 82.0%	0.65	0.15	↓ 77.4%
HKPU-FV	0.15	0.08	↓ 45.8%	0.21	0.20	↓ **05.7%**
IDIAP	0.63	0.15	↓ 75.8%	0.60	0.16	↓ 74.0%
SDUMLA-HMT	0.26	0.10	↓ 60.6%	0.32	0.21	↓ 35.0%

TABLE V
AVERAGE CORRELATION SCORE OF ORIGINAL AND DENOISED IMAGES

Additionally, to get a better sense of what denoising does to noise residuals, we visually compare the original PRNU to the PRNU of the denoised images in Fig. 5 [2]. What can be seen is that denoising causes characteristic structures to appear more prominent. As a result it seems most likely that regions with characteristic structures (highly correlated content) can have a huge impact on the sensor identification performance. Therefore, there are strong reasons to believe that PRNU estimates obtained from characteristic structures are not trustworthy.

VII. CONCLUSION

In this work, we studied the impact of highly correlated image content on the estimated PRNU of a single sensor unit and its impact on the sensor identification performance in the context of finger vein imagery. We showed formally and experimentally that in regions with characteristic, positionally stable structures (e.g, introduced by the finger positioning apparatus or the illumination pattern) the estimated PRNU is biased by the image content. Our results indicate that this bias (and so the choice of the image region) can have a huge impact on the sensor identification performance. Although we are not able to quantify the impact of the content due to a lack of visually similar-looking images captured with the different sensors, our work demonstrates that we need to be very careful about PRNU-based sensor identification results if image content is highly correlated (unfortunately this is very often the case for biometric datasets). Depending on the dataset composition, a bias of the PRNU with image content can even cause a false increase in sensor identification performance.

[2] For better readability please look at the figure in a digital version

REFERENCES

[1] F. Marra, G. Poggi, C. Sansone, and L. Verdoliva, "A deep learning approach for iris sensor model identification," *Pattern Recognition Letters*, vol. 113, pp. 46–53, 2018.

[2] C. Kauba, L. Debiasi, and A. Uhl, "Identifying the origin of iris images based on fusion of local image descriptors and prnu based techniques," in *Biometrics (IJCB), 2017 IEEE International Joint Conference on*. IEEE, 2017, pp. 294–301.

[3] L. Debiasi and A. Uhl, "Blind biometric source sensor recognition using advanced prnu fingerprints," in *Signal Processing Conference (EUSIPCO), 2015 23rd European*. IEEE, 2015, pp. 779–783.

[4] S. El-Naggar and A. Ross, "Which dataset is this iris image from?" in *WIFS*, 2015, pp. 1–6.

[5] N. Kalka, N. Bartlow, B. Cukic, and A. Ross, "A preliminary study on identifying sensors from iris images," in *Proceedings of the IEEE Conference on Computer Vision and Pattern Recognition Workshops*, 2015, pp. 50–56.

[6] A. Uhl and Y. Höller, "Iris-sensor authentication using camera prnu fingerprints," in *Biometrics (ICB), 2012 5th IAPR International Conference on*. IEEE, 2012, pp. 230–237.

[7] N. Bartlow, N. Kalka, B. Cukic, and A. Ross, "Identifying sensors from fingerprint images," in *Computer Vision and Pattern Recognition Workshops, 2009. CVPR Workshops 2009. IEEE Computer Society Conference on*. IEEE, 2009, pp. 78–84.

[8] D. Söllinger, B. Maser, and A. Uhl, "Prnu-based finger vein sensor identification: On the effect of different sensor croppings," in *Proceedings of the 12th IAPR/IEEE International Conference on Biometrics (ICB'19)*, 2019, pp. 1–8.

[9] J. Fridrich, "Sensor defects in digital image forensic," in *Digital Image Forensics*. Springer, 2013, pp. 179–218.
[10] J. Lukas, J. Fridrich, and M. Goljan, "Digital camera identification from sensor pattern noise," *IEEE Transactions on Information Forensics and Security*, vol. 1, no. 2, pp. 205–214, 2006.
[11] M. K. Mihcak, I. Kozintsev, and K. Ramchandran, "Spatially adaptive statistical modeling of wavelet image coefficients and its application to denoising," in *1999 IEEE International Conference on Acoustics, Speech, and Signal Processing. Proceedings. ICASSP99 (Cat. No. 99CH36258)*, vol. 6. IEEE, 1999, pp. 3253–3256.
[12] K. Dabov, A. Foi, V. Katkovnik, and K. Egiazarian, "Image denoising by sparse 3-d transform-domain collaborative filtering," *IEEE Transactions on image processing*, vol. 16, no. 8, pp. 2080–2095, 2007.
[13] Y. Yin, L. Liu, and X. Sun, "SDUMLA-HMT: A Multimodal Biometric Database," in *The 6th Chinese Conference on Biometric Recognition (CCBR 2011)*, ser. Springer Lecture Notes on Computer Science, vol. 7098, 2011, pp. 260–268.
[14] P. Tome, M. Vanoni, and S. Marcel, "On the vulnerability of finger vein recognition to spoofing," in *IEEE International Conference of the Biometrics Special Interest Group (BIOSIG)*, Sep. 2014. [Online]. Available: http://publications.idiap.ch/index.php/publications/show/2910
[15] M. S. M. Asaari and B. A. R. S. A. Suandi, "Fusion of band limited phase only correlation and width centroid contour distance for finger based biometrics," *Expert Systems with Applications*, vol. 41, no. 7, pp. 3367–3382, 2014.
[16] Y. Lu, S. J. Xie, S. Yoon, Z. Wang, and D. S. Park, "An available database for the research of finger vein recognition," in *Image and Signal Processing (CISP), 2013 6th InternationalCongress on Image and Signal Processing (CISP 2013)*, vol. 1. IEEE, 2013, pp. 410–415.
[17] C. Kauba, B. Prommegger, and A. Uhl, "Focussing the beam-a new laser illumination based data set providing insights to finger-vein recognition," in *2018 IEEE 9th International Conference on Biometrics Theory, Applications and Systems (BTAS)*. IEEE, 2018, pp. 1–9.
[18] P. Tome, M. Vanoni, and S. Marcel, "On the vulnerability of finger vein recognition to spoofingattacks," in *Proceedings of the International Conference of the Biometrics Special Interest Group (BIOSIG'14)*, Sep. 2014, pp. 111–120.
[19] B. Ton and R. Veldhuis, "A high quality finger vascular pattern dataset collected using acustom designed capturing device," in *International Conference on Biometrics, ICB 2013*. IEEE, 2013. [Online]. Available: http://doc.utwente.nl/87790/
[20] A. Kumar and Y. Zhou, "Human identification using finger images," *IEEE Transactions on Image Processing*, vol. 21, no. 4, pp. 2228–2244, 2012.
[21] C.-T. Li, "Source camera identification using enhanced sensor pattern noise," *IEEE Transactions on Information Forensics and Security*, vol. 5, no. 2, pp. 280–287, 2010.
[22] R. Caldelli, I. Amerini, F. Picchioni, and M. Innocenti, "Fast image clustering of unknown source images," in *2010 IEEE International Workshop on Information Forensics and Security*. IEEE, 2010, pp. 1–5.
[23] X. Lin and C.-T. Li, "Enhancing sensor pattern noise via filtering distortion removal," *IEEE Signal Processing Letters*, vol. 23, no. 3, pp. 381–385, 2016.
[24] ——, "Preprocessing reference sensor pattern noise via spectrum equalization," *IEEE Transactions on Information Forensics and Security*, vol. 11, no. 1, pp. 126–140, 2015.